International Journal of Solids and Structures 80 (2016) 445–455

Contents lists available at ScienceDirect

International Journal of Solids and Structures

journal homepage: www.elsevier.com/locate/ijsolstr

On interfacial energy of macroscopic domains in polycrystalline NiTi shape memory alloys

L. Dong [a,b], R.H. Zhou [a], X.L. Wang [c], G.K. Hu [d], Q.P. Sun [a,*]

[a] Department of Mechanical Engineering, The Hong Kong University of Science and Technology, Clear Water Bay, Hong Kong, China
[b] School of Civil Engineering, State Key Lab of Water Resources and Hydropower Engineering, Wuhan University, China
[c] School of Mechanical Engineering, University of Science and Technology Beijing, Beijing 100083, China
[d] Key Laboratory of Dynamics and Control of Flight Vehicle, Ministry of Education, School of Aerospace Engineering, Beijing Institute of Technology, Beijing 100081, China

ARTICLE INFO

Article history:
Received 31 May 2014
Revised 2 August 2015
Available online 19 October 2015

Keywords:
Phase transformation
Macroscopic domain
Interfacial or domain front energy
Effects of lengths and interface orientation

ABSTRACT

Under tension or tension/torsion combined loading, the formation and movement of macroscopic interfaces (domain fronts which separate the austenite and martensite regions) in the phase transition of a bulk fine-grained polycrystalline NiTi shape memory alloy (SMA) bar or tube specimen are well-observed phenomena. The interfacial energy of the macroscopic domain front, i.e., the energy per unit area of the front (interface), competes with the bulk energy of the system and plays an important role in understanding and modeling both equilibrium and non-equilibrium domain patterns. This paper investigates the physical origin of the interfacial energy of a planar interface and its orientation and length scale dependences in a bar structure. The energetics of a martensite domain with such a planar interface is quantified by using an elastic inclusion model. We show that the strain energy due to the presence of the martensite domain consists of two parts, the bulk energy (such as from bending) due to the constraints at the bar ends and the localized energy due to the mismatch between the spontaneous transformation strain of the domain and the surrounding austenite. The latter is stored around the domain front and is named as the interfacial energy (domain front energy). It is proved that the interface or the domain front of the bar prefers the orientation that minimizes the system total energy. This is supported by comparison with the experimental observation. The dependences of the interfacial energy on the bar geometry (bar thickness and width), the transformation strain and the interface orientation are quantified.

1. Introduction

The interfaces and their motion are widely observed in phase transformations in metals and ceramics such as the formation of dendrites in supercooled liquids (the molten material) and precipitates in alloys. The formation of interface takes place by a nucleation process of a new phase from its parent phase. The interfacial energy, i.e., the energy per unit area of the interface, is one of the most important quantities that affect the development of morphology and evolution of microstructure (Porter et al., 2009). For example, the variation of interface configuration (i.e., its orientation and area) and therefore the energy provides the driving force for many important kinetic processes of structure changes such as the formation of equilibrium microstructures, from twin structures, the shape of a grain to the macroscopic domain patterns in a polycrystal. NiTi shape memory alloy (SMA) is a typical material which can undergo diffusionless and displacive martensitic phase transformation and has many important applications. Extensive experimental researches have been performed on the deformation behavior of fine-grained polycrystalline NiTi SMAs (among many others, see Shaw and Kyriakides, 1997, 1998; Shaw, 2000; Zhang et al., 2010; Zhou, 2011 for bars, and see Li and Sun, 2002; Sun and Li, 2002; Feng and Sun, 2006; Zhou, 2011; Zhou and Sun, 2011 for tubes). For superelastic NiTi bars and tubes under stretching, a basic phenomenon of the deformation is the collective and localized phase transformation of the material and the resultant formation of macroscopic deformation domains as shown in Fig. 1. The low-strain (austenite) and high-strain (martensite) regions are separated by "sharp" interfaces (domain fronts) which orientate at about 35° to the transverse axis in a bar (see Fig. 1(a)) and at the middle part of the helix in a tube (see Fig. 1(b)). The high-strain domain consists of almost fully transformed grains whose statistical average transformation strains are 5% in axial direction and −2.5% in the other two directions (Li and Sun, 2002; Feng and Sun, 2006). The aforementioned interface orientation corresponds to the "invariant-line" on the bar or tube surface along which there is no in-plane misfit. Due to strong incompatibility of the deformation, the interface

* Corresponding author. Tel.: +852 2358 8655; fax: +852 2358 1543.
E-mail address: meqpsun@ust.hk (Q.P. Sun).

http://dx.doi.org/10.1016/j.ijsolstr.2015.10.006
0020-7683/

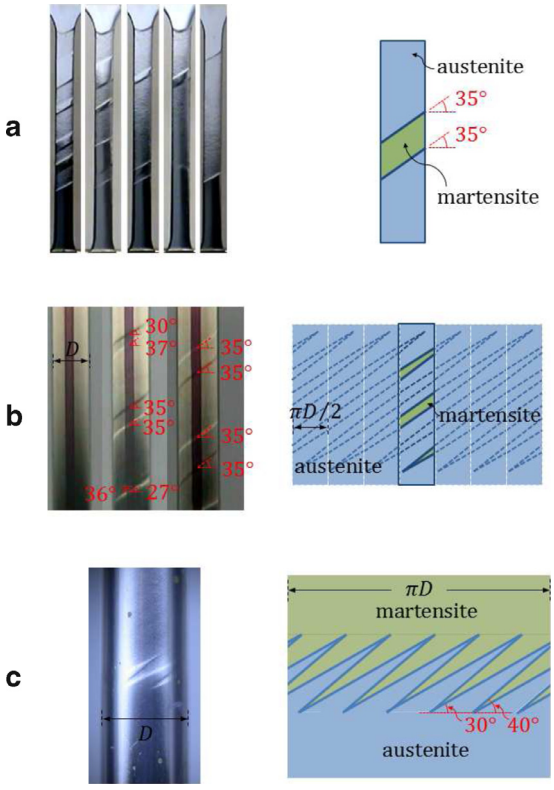

Fig. 1. Domain morphology and the interface (domain front) orientations in ultrafine-grained polycrystalline shape memory alloys under tensile stress: (a) the parallelogram domains in a strip geometry, (b) the helical domains in a tube geometry, (c) a cylindrical domain with branched fronts in a tube geometry.

orientation may also deviate from the "invariant-line" for the two end-tips of the helix (see Fig. 1(b)) and for the branched fronts (see Fig. 1(c)) in tubes. Preliminary researches show that the interfacial (domain front) energy plays an important role in determining the interface orientation. However, how to quantify the interfacial energy of the macroscopic domain and its orientation dependence still remain unsolved issues.

Although great advances have been achieved in modeling the interface and the interfacial energy at micro-scale (among many literatures, see Cahn and Hilliard, 1958; Khachaturyan, 1983; Roitburd, 1998; Maciejewski et al., 2005), relatively much less is known about the interfacial energy of the macroscopic domain in polycrystals. The key issues in understanding and modeling the macroscopic interface in bulk polycrystalline NiTi SMAs are the definition of interfacial energy in polycrystals, its physical nature and its orientation dependence. The formation of macroscopic interphase interfaces can be understood as follows. During stretching, the strong interactions among the phase transformation events of grains lead to the collective behavior of phase transition and the self-organization of these grains into a macroscopic domain (see Fig. 2). In terms of continuum mechanics, the deformation process of the material during phase transition involves intrinsic material instability at different length scales with complicated microstructure evolution. At the micro-scale, the crystal structure changes abruptly from a high-symmetry cubic lattice to a low-symmetry monoclinic lattice (Bhattacharya, 2003; see Fig. 2(e)). This cubic to monoclinic transformation leads to the twinned structures of martensite and forms an interface separating the twinned martensite from the parent lattice. Such interface of nanometer to micronmeter thickness is called the habit plane (see Fig. 2(c) and (d)). At the meso-scale, the microstructure of martensite has essential features related to crystallographic orientation. The microstructure of one grain can be very different from the neighboring

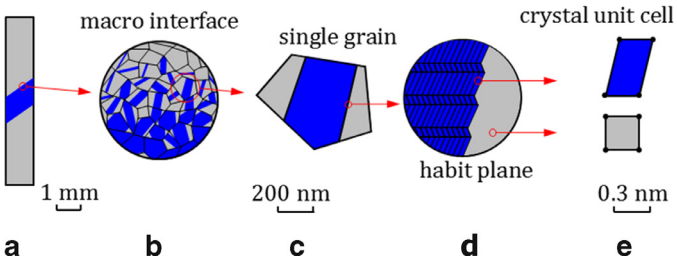

Fig. 2. Multi-scale structure of the interface (domain front) of a macroscopic domain and the material hierarchy of the domain front therein.

ones (see Fig. 2(b)). As the misfit presents, the formation of coherent interfaces raises the free energy of the system due to the elastic strain fields that arise. There is competition between the microstructure that each grain wants to form and the constraints that are imposed by the surrounding grains. In other words, the microstructure in one grain can affect the microstructure in another grain. As a consequence, a macroscopic interface (domain front) is formed at a length scale from a few microns to a few millimeters (see Fig. 2(a)). In previous works (Dong and Sun, 2009; He and Sun, 2009a, 2009b, 2010) the interface was treated to be a mathematically sharp surface and the interfacial energy was assumed to be a material constant. Later it was found that the interfacial energy (domain front energy) is mainly due to the transformation strain along the bar thickness or tube wall-thickness direction (He and Sun, 2009c; Dong and Sun, 2012) and the interfacial energy is linearly proportional to the bar thickness or wall-thickness. However, a more rigorous theoretical analysis based on analytics or numerical simulation is still missing. Therefore, it is of great interest for us to take the thickness effect into account and to systematically quantify the interfacial energy.

In general, similar to those for a microscopic interface, two modeling approaches of local (inclusion) model and nonlocal (gradient) model can be used to describe a macroscopic interface in NiTi SMAs. In the local (inclusion) model, the interface is taken as a mathematically sharp surface across which the strain suffers a jump from the low-strain (austenite) phase to the high-strain (martensite) phase (Dong and Sun, 2009). The interfacial energy density (per unit area) contains a length scale that is a measure of the physical thickness of the interface and is assumed to be evenly assigned to the whole interfacial area. In the nonlocal (gradient) model, the strain changes continuously but rapidly from high-strain to low-strain regions and the interfacial energy is in fact a bulk energy of the rapid transition regions which can be accounted for by a strain-gradient term in the energy function (Cahn and Hilliard, 1958; Cahn, 1961; Falk, 1983; He and Sun, 2009a, 2009b, 2010). In this gradient energy, a material length is introduced and used to describe the length scale of microstructure features such as the interface thickness at micro- or nano-scale. It is clear that both local and nonlocal approaches have clear physical meanings but are mathematically different. The nonlocal model has become a preferred method to describe complex domain patterns due to its computational advantages (e.g., no singularity and no mesh-dependence), but in understanding basic phenomena like the interfacial energy, the local model has advantage due to its simplicity.

The objective of this paper is to study the interface structure and to define the interfacial energy of macroscopic domains in polycrystalline NiTi shape memory alloys by using a local (inclusion) model. We focus on the energetics of a martensite domain with a single planar interface in bars of different length, width and thickness and aim to clarify the physical origin of the interfacial energy and quantify its length and orientation dependence. The paper is organized as follows. In Section 2, the physical origin of interfacial energy is discussed by an analysis of strain compatibility at the interface (domain front). In Section 3, the equilibrium (or energy minimized) domain and its

interface orientation are determined by means of finite element computation and compared with experimental data. In Section 4, the approximate expression of interfacial energy is derived and its length dependence is quantified. In Section 5, the orientation dependence of interfacial energy is discussed. The summary and conclusions are given in Section 6.

2. Strain mismatch and interfacial energy

During the phase transformation of polycrystalline NiTi shape memory alloys, the formation of new martensite phase in some macroscopic region of initial austenite phase is accompanied by a change in the shape of this region, which can be represented by a symmetric transformation strain ε_{ij}^{p}. Due to the constraint of the initial phase, the new phase tends to choose a certain preferred shape and orientation (Roitburd, 1969, 1974, 1978; Boyko et al., 1994). In this section, we shall present the strain mismatch between these two phases and the resultant interfacial energy.

The problem consists of finding displacement u_i, strain ε_{ij} and stress σ_{ij} at an arbitrary point x_i inside the solid. The total strain ε_{ij} is regarded as the sum of elastic strain ε_{ij}^{e} and transformation strain ε_{ij}^{p},

$$\varepsilon_{ij} = \varepsilon_{ij}^{e} + \varepsilon_{ij}^{p}, \tag{1}$$

where $\varepsilon_{ij} = (u_{i,j} + u_{j,i})/2$ with $u_{i,j} = \partial u_i/\partial x_j$.

We assume that during the phase transformation the displacements at all points of the solid are continuous and the total strains are compatible. The condition of compatibility of strains at any point inside the solid (St. Venant condition) can be expressed in the following form (Roitburd, 1978; Mura, 1987; Boyko et al., 1994):

$$R_{ij} = e_{ilm}e_{jpq}\varepsilon_{mq,lp} = 0, \tag{2}$$

where e_{ilm} is the permutation tensor. The tensor R_{ij} is known as the incompatibility tensor.

The gradient term $\varepsilon_{mq,\,lp}$ is continuous inside each phase but discontinuous at the interface between the two phases. The jump across the interface can be written as

$$[\varepsilon_{mq,lp}] = \varepsilon_{mq.lp}(\text{austenite}) - \varepsilon_{mq.lp}(\text{martensite}) = [\varepsilon_{mq}]n_l n_p, \tag{3}$$

where $[\varepsilon_{mq}] = \varepsilon_{mq}(\text{austenite}) - \varepsilon_{mq}(\text{martensite})$ is the jump magnitude of the total strain and n_l is a unit vector along the normal to the investigated part of the interface.

For those points located at the interface, the strain compatibility condition in Eq. (2) can be shown as:

$$\left[R_{ij}\right] = e_{ilm}e_{jpq}[\varepsilon_{mq}]n_l n_p = 0. \tag{4}$$

Substituting Eq. (1) into Eq. (4), we have

$$\left[R_{ij}^{e}\right] = e_{ilm}e_{jpq}\left[\varepsilon_{mq}^{e}\right]n_l n_p = e_{ilm}e_{jpq}\varepsilon_{mq}^{p}n_l n_p, \tag{5}$$

with

$$\begin{aligned}
[R_{11}^{e}] &= \varepsilon_{33}^{p}n_2^2 + \varepsilon_{22}^{p}n_3^2 - 2\varepsilon_{23}^{p}n_2n_3,\\
[R_{22}^{e}] &= \varepsilon_{33}^{p}n_1^2 + \varepsilon_{11}^{p}n_3^2 - 2\varepsilon_{13}^{p}n_1n_3,\\
[R_{33}^{e}] &= \varepsilon_{22}^{p}n_1^2 + \varepsilon_{11}^{p}n_2^2 - 2\varepsilon_{12}^{p}n_1n_2,\\
[R_{12}^{e}] &= [R_{21}^{e}] = -\varepsilon_{33}^{p}n_1n_2 - \varepsilon_{12}^{p}n_3^2 + \varepsilon_{13}^{p}n_2n_3 + \varepsilon_{23}^{p}n_1n_3,\\
[R_{13}^{e}] &= [R_{31}^{e}] = -\varepsilon_{22}^{p}n_1n_3 + \varepsilon_{12}^{p}n_2n_3 - \varepsilon_{13}^{p}n_2^2 + \varepsilon_{23}^{p}n_1n_2,\\
[R_{23}^{e}] &= [R_{32}^{e}] = -\varepsilon_{11}^{p}n_2n_3 + \varepsilon_{12}^{p}n_1n_3 + \varepsilon_{13}^{p}n_1n_2 - \varepsilon_{23}^{p}n_1^2.
\end{aligned}$$

A simple geometrical interpretation may be given to Eq. (4). The preservation of the coherence on the interface means that each vector X_j that connects some two points on the interface before the phase transformation passes into the same vector after the phase transformation, regardless with which contacting phase it is considered to belong, i.e.,

$$\left[u_{i,j}\right]X_j = 0, \tag{6}$$

where $u_{i,j}$ is the displacement gradients (total distortions) of the contacting phases relative to the initial single-phase state. If we consider a plane interface element with the normal n_j, then $X_j n_j = 0$ and the requirement for the preservation of the contact in Eq. (6) is fulfilled if

$$\left[u_{i,j}\right] = s_i n_j, \tag{7}$$

where s_i is the magnitude of the jump to be determined. $[u_{i,j}]$ describes the distortion with an invariant plane. All the planes with the normal n_j are not distorted since the displacements in each plane are the same, $u_i = s_i x$, x being the distance of the plane from the interface. Under the condition in Eq. (7), the relative strain of the contacting phases is reduced to a simple shear and a normal displacement of the stack of planes parallel to the interface.

The compatibility preservation condition in Eq. (7) can be reduced to definite restrictions on permissible strain discontinuity and disorientation:

$$\left[\varepsilon_{ij}\right] = \left[\varepsilon_{ij}^{e}\right] - \varepsilon_{ij}^{p} = \frac{1}{2}\left(s_i n_j + s_j n_i\right), \tag{8}$$

$$\left[\omega_{ij}\right] = \left[\omega_{ij}^{e}\right] - \omega_{ij}^{p} = \frac{1}{2}\left(s_i n_j - s_j n_i\right), \tag{9}$$

where ω_{ij}^{p} is the antisymmetric parts of the transformation strain which is taken as zero in our study. The rotation jump (in addition to the transformation strain) of a domain in a long strip in tension creates a slight misalignment (kinking) with the loading axis and thus causes bending (Corona et al., 2002) and it is ignored here for the purpose of simplicity of mathematical analysis. The effect of kinking on energetics is definitely worth investigation in the future work. The strain discontinuity in Eq. (8) is a solution to the compatibility condition in Eq. (4).

If we have $\varepsilon_{ij}^{p} = -(s_i n_j + s_j n_i)/2$ (or equivalently $[R_{ij}^{e}] = 0$), then the two phases contact along a non-distorted common plane (invariant plane) and no elastic strain arises as a result of the contact of phases (see Fig. 3). On the contrary, the deviation of transformation strain discontinuity from the invariant plane defines the degree of mutual elastic phase distortions and gives rise to internal stresses. In other words, it is the interface incompatibility of transformation strain on the interphase boundary that is the source of the internal stresses in a heterophase system. The fields of internal stresses are long range and are spread from the source interface to distances of the order of the boundary extent (the smallest dimension of the object) (Roitburd, 1978). For example, in Dai and Cai (2006) the analytical solution for an infinite slender elastic cylinder under phase transition was presented and it was found that the thickness of the phase boundary is proportional to the radius of the cylinder. But for most general problems, it is extremely challenging to achieve analytical solutions and we have to implement numerical solutions such as finite element simulations.

For most shape memory alloys under tensile loading, the non-zero components are only ε_{11}^{p}, ε_{22}^{p} and ε_{33}^{p}. Then Eq. (5) can be simplified

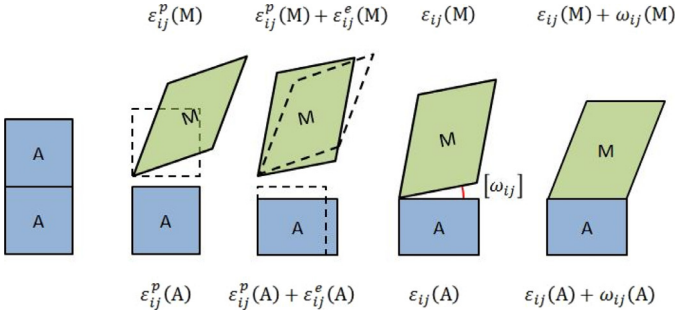

Fig. 3. Model for defining strain compatibility on an interface (**A** for austenite and **M** for martensite).

as:

$$[\boldsymbol{R}^e] = \begin{bmatrix} \varepsilon^p_{33} n_2^2 + \varepsilon^p_{22} n_3^2 & -\varepsilon^p_{33} n_1 n_2 & -\varepsilon^p_{22} n_1 n_3 \\ -\varepsilon^p_{33} n_1 n_2 & \varepsilon^p_{33} n_1^2 + \varepsilon^p_{11} n_3^2 & -\varepsilon^p_{11} n_2 n_3 \\ -\varepsilon^p_{22} n_1 n_3 & -\varepsilon^p_{11} n_2 n_3 & \varepsilon^p_{22} n_1^2 + \varepsilon^p_{11} n_2^2 \end{bmatrix}. \tag{10}$$

It can be checked that in Eq. (10) there is no specific interface orientation n_l that can satisfy the condition $[R^e_{ij}] = 0$. We can expect that the elastic strain and stress field have to appear around the interface to guarantee the compatibility of total strains. As a consequence, it will lead to the interfacial energy stored around the interface.

In previous studies of thin-walled structures like thin-walled tubes (Li and Sun, 2002; He and Sun, 2009a, 2009b, 2009c), only two transformation strain components (ε^p_{11} and ε^p_{33}) were considered in determining the orientation of the domain front in the x_1x_3-plane. The transformation strain ε^p_{22} along the wall-thickness direction (x_2-axis) was treated separately and considered as the origin of interfacial energy. In this case we can ignore the effect of ε^p_{22} and n_2 in Eq. (10):

$$[\boldsymbol{R}^e] = \begin{bmatrix} 0 & 0 & 0 \\ 0 & \varepsilon^p_{33} n_1^2 + \varepsilon^p_{11} n_3^2 & 0 \\ 0 & 0 & 0 \end{bmatrix}. \tag{11}$$

It can be seen that we have $[R^e_{ij}] = 0$ for two specific orientations n_l of the "invariant-line" on the x_1x_3-plane:

$$\mathbf{n} = \left[\pm \sqrt{-\frac{\varepsilon^p_{11}}{\varepsilon^p_{33} - \varepsilon^p_{11}}} \; 0 \; \sqrt{\frac{\varepsilon^p_{33}}{\varepsilon^p_{33} - \varepsilon^p_{11}}} \right]. \tag{12}$$

Therefore, the "invariant-line" exists only if ε^p_{11} and ε^p_{33} have opposite signs ($\varepsilon^p_{33} > 0 > \varepsilon^p_{11}$). The corresponding orientation angle θ to the x-axis can be given as:

$$\theta = \tan^{-1}\left(\sqrt{-\frac{\varepsilon^p_{11}}{\varepsilon^p_{33}}} \right) \text{ or } \theta = \pi - \tan^{-1}\left(\sqrt{-\frac{\varepsilon^p_{11}}{\varepsilon^p_{33}}} \right). \tag{13}$$

For the transformation strain $\varepsilon^p_{11} = -2.5\%$ and $\varepsilon^p_{33} = 5\%$ in polycrystalline NiTi shape memory alloys, the orientation angle $\theta_0 \approx 35°$. In Li and Sun (2002), the principle of energy minimization was applied to determine the orientation angle of a thin flat ellipsoidal domain in the tube system, and the same interface orientation was found as those in Eqs. (12) and (13).

Comment 1: Anisotropy widely exists in most of textured polycrystalline materials. Here we made the assumptions of isotropic transformation strains and isotropic linear elastic austenite and martensite. The purpose is mainly for the simplicity of mathematical analysis. The effects of material anisotropy on the interfacial energy of domain are definitely worth investigation in the future work.

Next, we aim to study the effect of the transformation strain $\varepsilon^p_{22}(= -2.5\%)$ along the wall-thickness direction (x_2-axis) and get preliminary understanding of interfacial energy. This target can be achieved by considering a simple plane-stress problem of an infinite long bar in x_3x_2-plane with a half ($x_3 < 0$) in austenite phase and the other half ($x_3 > 0$) in martensite phase as shown in Fig. 4. The thickness of the bar (along x_2-axis) is $2c$. The original problem in Fig. 4(a) can be decomposed into three sub-problems as shown in Fig. 4(b)–(d) and the solutions are given in Appendix A. The distributions of total stresses along x_3-axis for those points located at $x_2 = 0$ (see Eq. (A11) in Appendix A) can be expressed as

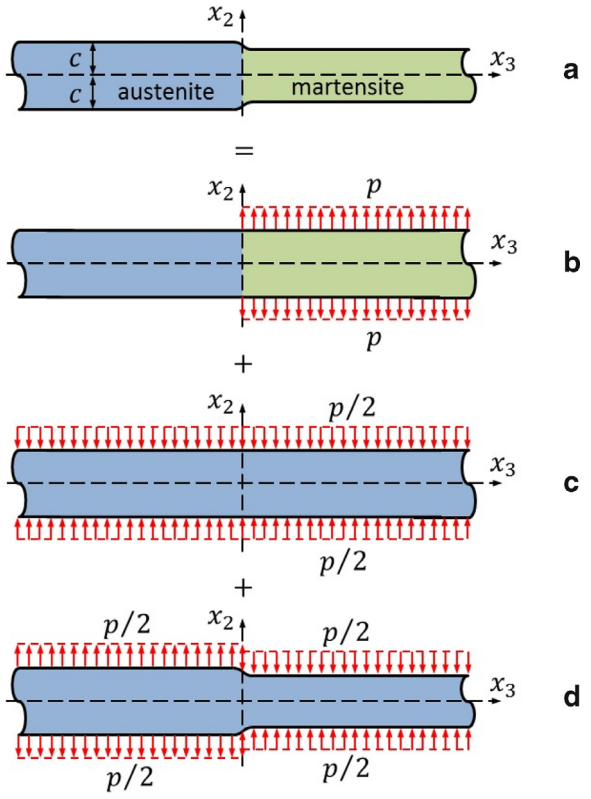

Fig. 4. An infinite bar with a martensite inclusion and the decomposition of the original problem into three sub-problems: (a) original problem, (b) sub-problem I, (c) sub-problem II, (d) sub-problem III.

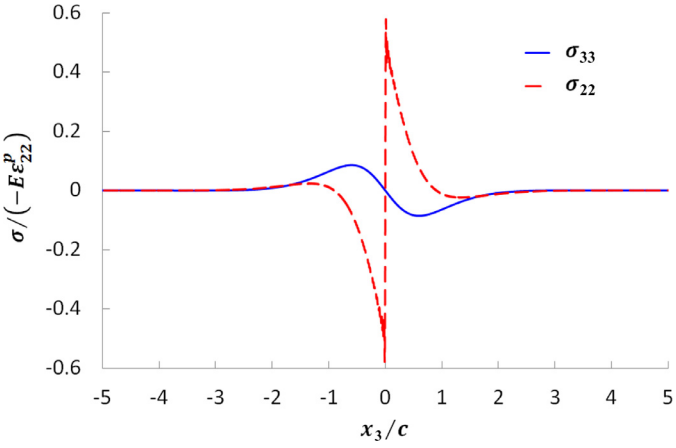

Fig. 5. The variation of stresses σ_{33} and σ_{22} along the x_3-axis when $x_2 = 0$.

$$\begin{aligned} \sigma_{33} &= \frac{E\varepsilon^p_{22}}{\pi} \int_0^\infty \frac{\sinh k - k\cosh k}{\sinh k \cosh k + k} \frac{\sin\left(\frac{kx_3}{c}\right)}{k} dk, \\ \sigma_{22} &= -\frac{E\varepsilon^p_{22}}{\pi} \int_0^\infty \left(1 - \frac{\sinh k + k\cosh k}{\sinh k \cosh k + k}\right) \frac{\sin\left(\frac{kx_3}{c}\right)}{k} dk, \\ \sigma_{32} &= 0. \end{aligned} \tag{14}$$

The variation of stresses σ_{33} and σ_{22} in Eq. (14) along x_3-axis is plotted in Fig. 5. It is seen that the stresses are mainly concentrated in a small region ($|x_3/c| < 1$) around the austenite–martensite interface. It is stress free for the regions far away from the interface and therefore they have no contribution to the interfacial energy.

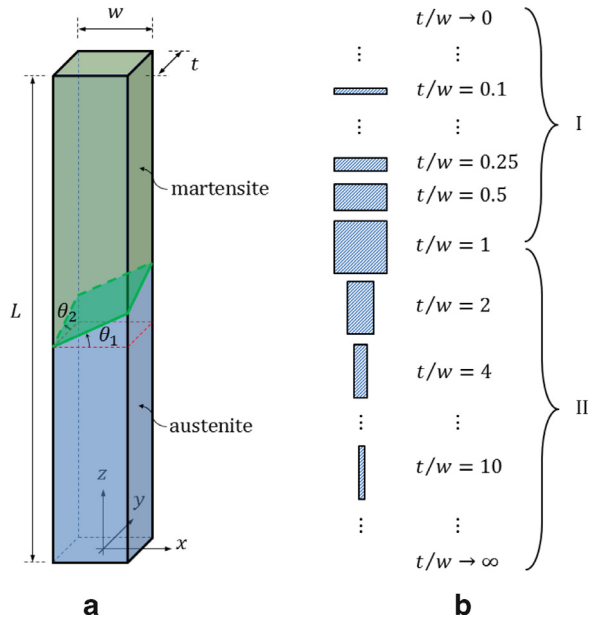

Fig. 6. A straight bar of rectangular cross-section. The bar consists of high-strain (martensite) and low-strain (austenite) regions that are separated by a single planar interface with orientation angles θ_1 and θ_2.

The elastic strain energy of the bar (see Eq. (A12) in Appendix A) can be approximately written as

$$U_{\text{el}} = \frac{E\left(\varepsilon_{22}^{p}\right)^{2} c}{\pi} \int_0^{\infty} \left\{ \int_0^{\infty} \left[1 - \frac{2\sinh k \sinh k}{\sinh k \cosh k + k} \frac{1}{k} \right] \frac{\sin\left(\frac{kx_3}{c}\right)}{k} dk \right\} dx_3. \tag{15}$$

Although Eq. (15) is still not very simple, we can see that the elastic strain energy U_{el} is linearly proportional to the half-width c along x_2-axis and this energy is mainly stored around the austenite–martensite interface.

As a summary, it is clearly shown in Eq. (10) that the strain mismatch due to the transformation strain in a polycrystalline NiTi bar cannot be accommodated without elastic strains and therefore the elastic stresses must appear around the interface. Such a localized stress field leads to the interfacial energy (see Eq. (15) as an example) for the macroscopic austenite–martensite interface. This physical picture and origin of the macroscopic interface energy is consistent with the thermodynamic Ginzburg-Landau theory (or Cahn and Hilliard theory) in that the interface zone is in the non-convex region of free energy function and has extra bulk energy than the austenite and martensite phases.

3. Interface orientations in bars under tension

In this section, we shall determine the interface orientations in superelastic NiTi bars under tensile loading. We consider a rectangular bar of a length L having a uniform cross-section (width w and thickness t) as shown in Fig. 6. We assume that half of the bar is transformed into the martensite phase (domain Ω) with a planar austenite–martensite interface located at the center of the bar. The assumption of such a planar interface is motivated by both the experimental observation and the purpose of mathematical simplicity.

Based on the understanding in Section 2, the problem to quantify the interfacial energy can be solved by first determining the two orientation angles (θ_1 and θ_2) of the austenite–martensite interface (see Fig. 6). The total energy of the system is computed by means of finite element modeling. We aim to find the interface orientation (θ_1 and θ_2) of an energy minimized configuration for various bar width w and thickness t. For simplicity, we assume the martensite phase and the austenite phase have the same elastic constants (modulus $E = 30$ GPa and Poisson's ratio $\nu = 0.3$). The volume change in phase transformation can be ignored and the nonzero components can be written as $\varepsilon_{11}^{p} = \varepsilon_{22}^{p} = -2.5\%$, $\varepsilon_{33}^{p} = -2\varepsilon_{11}^{p} = 5\%$.

The Helmholtz free energy of the system under the displacement-controlled boundary conditions can be expressed as (Dong and Sun, 2012):

$$U_{\text{total}} = \Delta U_{\text{chem}} + U_{\text{el}} + U_{\text{ext}}, \tag{16}$$

where ΔU_{chem} is the change in chemical free energy, U_{el} is the strain energy due to the presence of martensite domain and U_{ext} is the extra elastic energy due to the external displacement-controlled stretching.

Taking the stress-free austenite phase as the reference state, the total change in chemical free energy due to the thermo-elastic martensitic transformation is

$$\Delta U_{\text{chem}} = V_{\Omega} \Delta\varphi(T) = \frac{L}{2} wt \Delta\varphi(T), \tag{17}$$

where V_{Ω} is the volume of martensite and $\Delta\varphi(T)$ is the chemical free energy density difference between two phases. It only depends on the temperature T and can be approximated as a linear function of T around the equilibrium temperature T_0:

$$\Delta\varphi(T) = \varphi^{M}(T) - \varphi^{A}(T) = k(T - T_0), \tag{18}$$

where k is a material constant determined by the experiments.

The strain energy due to the presence of the martensite domain Ω can be expressed as

$$U_{\text{el}} = -\frac{1}{2}\left(\bar{\sigma}_{11}\varepsilon_{11}^{p} + \bar{\sigma}_{22}\varepsilon_{22}^{p} + \bar{\sigma}_{33}\varepsilon_{33}^{p}\right) V_{\Omega}, \tag{19}$$

where $\bar{\sigma}_{11}$, $\bar{\sigma}_{22}$ and $\bar{\sigma}_{33}$ denote the average of the stress σ_{11}, σ_{22} and σ_{33}, respectively over Ω:

$$\bar{\sigma}_{11} = \frac{1}{V_{\Omega}} \int_{\Omega} \sigma_{11} dV, \ \bar{\sigma}_{22} = \frac{1}{V_{\Omega}} \int_{\Omega} \sigma_{22} dV, \ \bar{\sigma}_{33} = \frac{1}{V_{\Omega}} \int_{\Omega} \sigma_{33} dV, \tag{20}$$

The extra elastic energy due to external displacement-controlled loading can be expressed as

$$U_{\text{ext}} = Lwt \frac{E}{2} \left(\varepsilon_0 - \frac{\varepsilon_{33}^{p}}{2} \right)^2, \tag{21}$$

where ε_0 is the applied nominal strain.

For our problem, the total change in chemical free energy ΔU_{chem} in Eq. (17) is fixed. For a given nominal strain, the extra elastic energy U_{ext} in Eq. (21) is also fixed. Therefore, we only need to investigate the strain energy U_{el} due to the presence of the martensite domain (see Eq. (19)). In the finite element modeling, the boundary constraints can be set as follows: at the upper surface ($z = L$), the deformation along the z-axis is forbidden ($u_3 = 0$) and especially at the center of the upper surface ($x = y = 0,\ z = L$) the deformations along the x- and y-axes are also forbidden due to symmetry ($u_1 = u_2 = 0$). At the bottom surface ($z = 0$), the deformations along the x- and y-axes are forbidden due to symmetry ($u_1 = u_2 = 0$), and the elongation along the z-axis is free ($u_3 \neq 0$) and its magnitude is the same for all surface points.

We first choose the bar geometry as $L = 20$ mm and $w = 1$ mm. The variation of strain energy U_{el} with two orientation angles θ_1 and θ_2 for four different bar thickness/width ratio ($t/w = 0.25,\ 0.5,\ 0.75,\ 1$) is shown in Fig. 7. It is seen that the minimum strain energy always occurs at the same orientation angles ($\theta_1 \approx 35°$ and $\theta_2 \approx 0°$). In other words, the interface tends to orient along the "invariant-line" on the front surface (xz-plane) of the bar, while the side-walls of the interface (on yz-surface) are always perpendicular to the loading axis (z-axis). It is noticed that for the case of a square

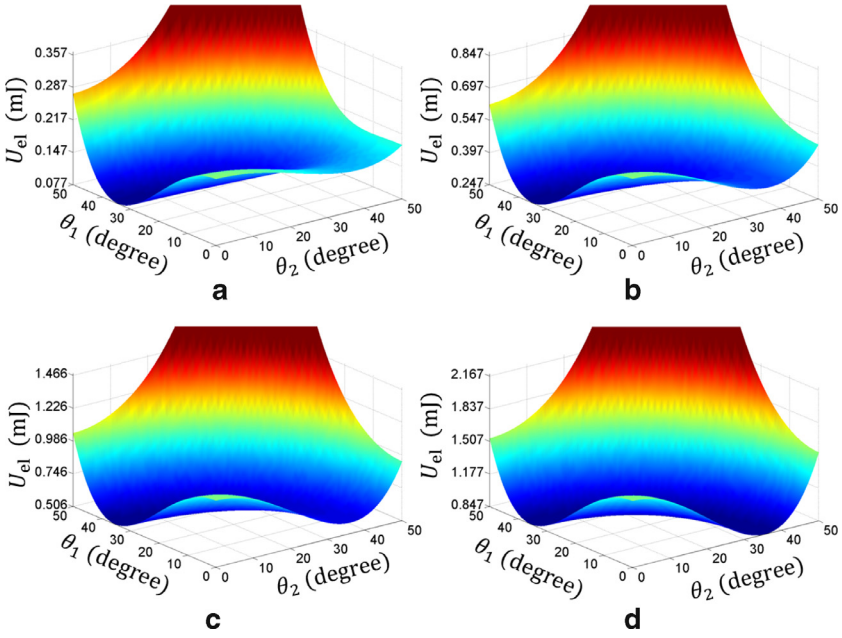

Fig. 7. The variation of total energy U_{el} with two orientation angles θ_1 and θ_2 for different bar thickness/width ratio: (a) $t/w = 0.25$, (b) $t/w = 0.5$, (c) $t/w = 0.75$, (d) $t/w = 1$ (all with given $L/w = 20$).

cross-section (with $t/w = 1$), there exists another pair of orientation angles ($\theta_1 \approx 0°$ and $\theta_2 \approx 35°$) corresponding to the minimum total energy due to the symmetry.

Experimental observation of morphologies of austenite–martensite interfaces was conducted for uni-axially stretched NiTi shape memory alloy bars of different aspect ratios ranging from 0.25 to 1. As shown in Fig. 8, the interface on the front surface (xz-plane) of each bar oriented at around 35° to the x-axis, while the interface on the side surface (yz-plane) of each bar was always perpendicular to the loading axis (z-axis). Such experimental observations agree well with our modeling predications.

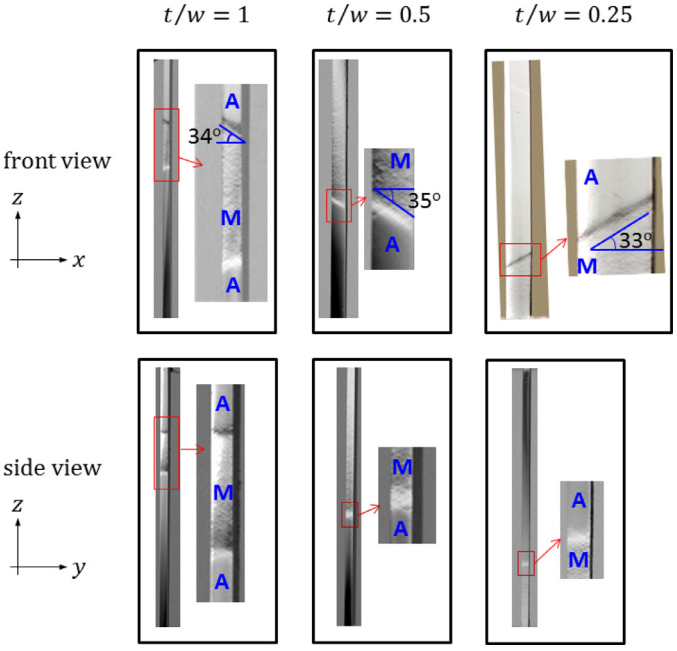

Fig. 8. Morphologies of interfaces (domain fronts) between austenite and martensite in uni-axially stretched NiTi shape memory alloy bars of different aspect ratios (t/w = 1.0, 0.5, 0.25, 0.1).

As a summary, for long NiTi bars (with $L \gg w$) under stretching, the orientation angles of the interface should always be $\theta_1 = \theta_0 \approx 35°$ and $\theta_2 \approx 0°$.

4. Interfacial energy and its length dependence

In this section, we shall derive the approximate expression of the interfacial energy. Based on the analysis and experimental observation in Section 3, we recognize that the two orientation angles of the interface are always $\theta_1 = \theta_0 \approx 35°$ and $\theta_2 \approx 0°$ for long NiTi bars (with $L \gg w$). Therefore, in this section our focus will be on the three length scales (bar length L, width w and thickness t).

For the cases with displacement-controlled boundary constraints studied in Section 3, the strain energy U_{el} (see Eq. (19)) consists of two parts, the interfacial energy and the bulk bending energy. The interfacial energy is due to the mismatch between the spontaneous transformation strain of the domain and the surrounding austenite and is localized around the domain front (interface), while the bulk bending energy is due to the constraints at the bar ends and is stored throughout the whole bar. To get a clear understanding of the interfacial energy, we first choose different boundary constraints from those in Section 3 to remove the bulk bending energy: at the upper surface ($z = L$), the deformations are totally free ($u_1 \neq 0, u_2 \neq 0, u_3 \neq 0$). At the bottom surface ($z = 0$), the deformations are all forbidden ($u_1 = u_2 = u_3 = 0$).

The variation of the interfacial energy density per unit area $U_{front}/(tw/\cos\theta_0)$ with the bar thickness t and width w is shown in Fig. 9. It is seen that the interfacial energy density $\gamma = U_{front}/(tw/\cos\theta_0)$ is linearly proportional to the bar thickness t and does not depend on the specific value of the bar width w:

$$U_{front} = \gamma \frac{wt}{\cos\theta_0} = C_2 t \frac{wt}{\cos\theta_0}, \tag{22}$$

where C_2 is a constant.

From Eq. (22) it is seen that there exists a characteristic length scale $l_{front} \sim t$. To clarify this length scale, the distributions of the normal strain ε_{22} across the interface along z-axis for those points located at $x = y = 0$ are plotted in Fig. 10. It is seen that the length scale l_{front} is linearly proportional to the bar thickness t. This confirms

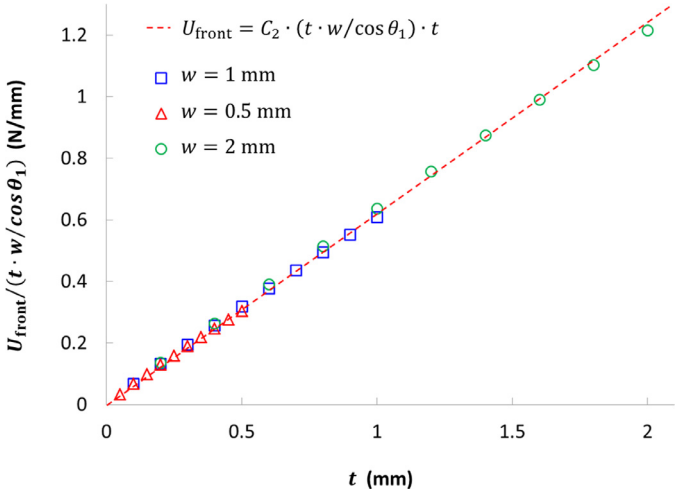

Fig. 9. The variation of the front energy density per unit area $U_{\text{front}}/(t \cdot w/\cos\theta_0)$ with the bar thickness t and width w.

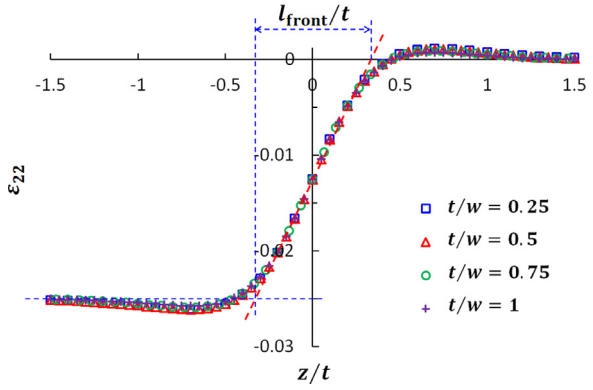

Fig. 10. The distribution of the normal strain ε_{22} along the z-axis for those points located at $x = y = 0$.

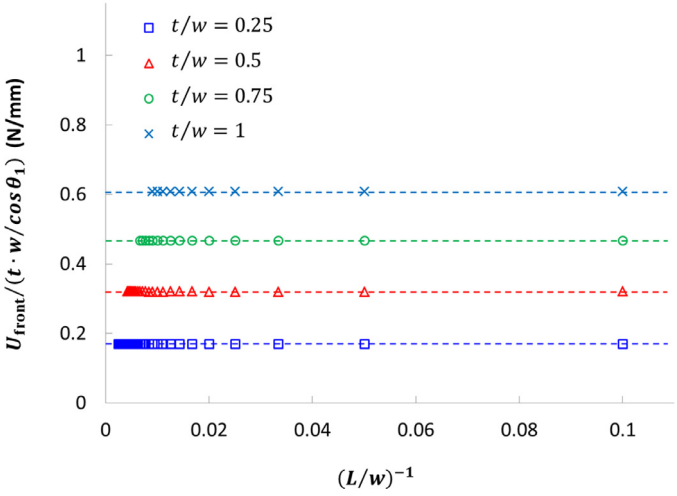

Fig. 11. The variations of the front energy density per unit area $U_{\text{front}}/(t \cdot w/\cos\theta_0)$ with the normalized bar length L/w for different normalized bar thickness (t/w = 0.25, 0.5, 0.75, 1).

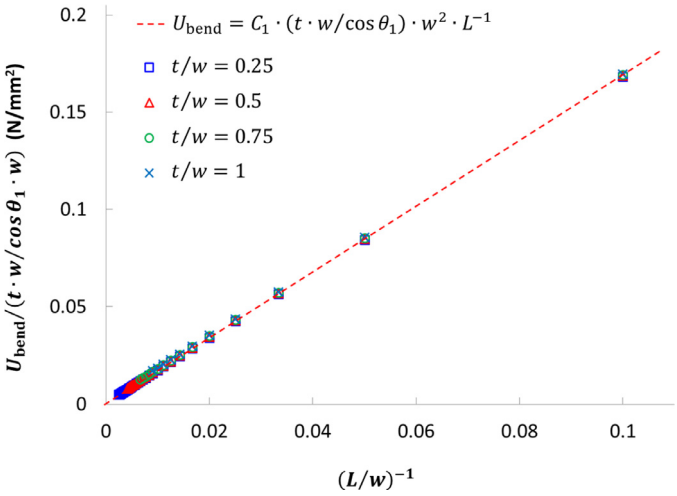

Fig. 12. The variations of (a) the bending energy U_{bend} and (b) the front energy density per unit area $U_{\text{front}}/(t \cdot w/\cos\theta_0)$ with the normalized bar length L/w for different normalized bar thickness (t/w = 0.25, 0.5, 0.75, 1).

the statement in Section 2 that the interfacial energy U_{front} is a local elastic energy stored around the domain front (interface).

From Eqs. (15) and (19), we notice that the transformation strains ε_{11}^p and ε_{33}^p show no contribution to the strain energy U_{el} since the interface orientation $\theta_1 = \theta_0 \approx 35^\circ$ largely reduces the xz-plane mismatch. Therefore, we can draw the conclusion that the interfacial energy is fully due to the transformation strain ε_{22}^p along the bar thickness direction:

$$U_{\text{front}} = -\frac{1}{2}\tilde{\sigma}_{22}\varepsilon_{22}^p V_\Omega. \tag{23}$$

Next, we consider the displacement-controlled loading condition to check if the end constraint and the bar length L contribute to the interfacial energy. The variation of the interfacial energy density per unit area $U_{\text{front}}/(tw/\cos\theta_0)$ with the normalized bar length L/w for different normalized bar thickness (t/w = 0.25, 0.5, 0.75, 1) are shown in Fig. 11. It is seen that the interfacial energy density $U_{\text{front}}/(tw/\cos\theta_0)$ does not depend on the normalized bar length L/w, which double confirms our conclusion that the interfacial energy (domain front energy) is a local elastic energy due to the local stress field around the domain front.

The variation of the bending energy U_{bend} with the normalized bar length L/w for different normalized bar thickness (t/w = 0.25, 0.5, 0.75, 1) are shown in Fig. 12. It is seen that the normalized bending energy $U_{\text{bend}}/(tw/\cos\theta_0 w)$ is inversely proportional to the normalized bar length L/w and does not depend on the normalized bar thickness t/w:

$$U_{\text{bend}} = C_1 \frac{wt}{\cos\theta_0}\frac{w^2}{L}, \tag{24}$$

where C_1 is a constant. The bending energy U_{bend} therefore is a bulk elastic energy since it depends on the bar length L.

As a summary, for long NiTi bars (with $L \gg w$) under stretching, the interfacial energy (domain front energy) is a local elastic energy due to the local stress field around the domain front. The interfacial energy density γ does not depend on the bar length L and width w, while it is linearly proportional to the bar thickness t.

5. Orientation dependence of the interfacial energy

Recent experiments on a simply supported NiTi shape memory alloy bar under three-point bending (with a concentrated force applied at the center of the bar) demonstrate that there was orientation (the angle θ to the vertical axis of the bar) evolution of the interface between austenite matrix and quasi-isosceles-triangle shaped martensite domain (see Fig. 13). At the beginning of the martensite domain nucleation, the interface was oriented at about 35° (see Fig. 13(a)) to the vertical axis of the bar, similar to the "invariant line" in tension

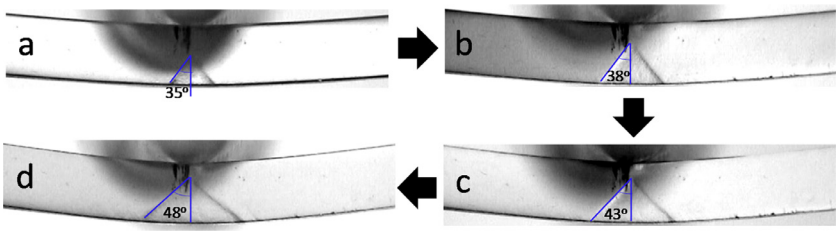

Fig. 13. The orientation (the angle to the vertical axis of the bar θ) evolution of the interface between austenite matrix and quasi-isosceles-triangle shaped martensite domain in a simply supported NiTi shape memory alloy bar under three-point bending: (a) 35°; (b) 38°; (c) 43°; (d) 48°.

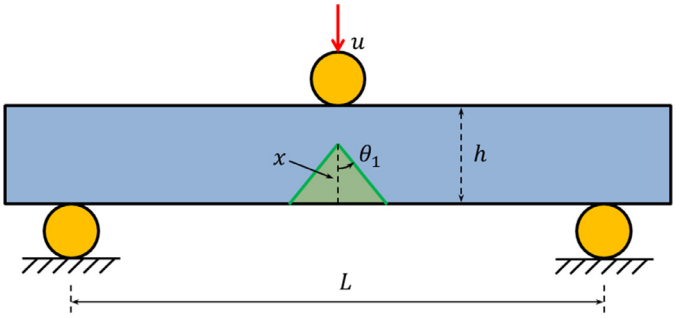

Fig. 14. A straight bar of rectangular cross-section under three-point bending. The bar consists of high-strain (martensite) and low-strain (austenite) regions that are separated by planar interfaces.

of bars. For the quasi-isosceles-triangle shaped domain under continued bending, in addition to the upward propagation of the apex, the interfaces gradually rotate which leads to an increase of the orientation angle θ (35°→38° → 43° → 48°). The martensite domain growth through interface rotation significantly reduced the curvature of bended shape of the transformed zone due to the physical origin of the transformation strain in the longitudinal direction, thus releasing the bending strain energy. From an energetic point of view, the rotation of the interface associated with martensite domain growth can be regarded as the result of the energy minimization principle.

Consider the three-point bending model shown in Fig. 14. We choose the bar geometry as $L = 20$ mm and $h = 1$ mm. For this model, there are two governing parameters: the height x of the martensite domain and the orientation angle θ_1. The total energy of the system is also computed by means of finite element modeling. We aim to find the energy minimized configuration for various given displacement u. The phase transformation strain is the same as that for the tensile loading in Section 3 with $\varepsilon^p_{11} = \varepsilon^p_{22} = -2.5\%$, $\varepsilon^p_{33} = -2\varepsilon^p_{11} = 5\%$.

The variation of total energy U_{total} with two governing parameters x/h and θ_1 for four different applied loads ($u/h = 1,\ 1.2,\ 1.4,\ 1.6$) is shown in Fig. 15. For relatively small displacement $u = h$, the energy minimized configuration corresponds to the fully austenite phase. For $u = 1.2h$, the orientation angle θ_1 for the energy minimized configuration is about 35°. It is seen that this preferred orientation angle θ_1 gradually increases as the applied displacement u increases. At the same time, the height x of the martensite domain also increases as u increases.

When the interface orientation θ_1 deviates from 35°, the interfacial energy U_{front} will not only depend on the transformation strain ε^p_{22} along the bar thickness direction (see Eq. (23)), but also will depend on the other two transformation strains (ε^p_{11} and ε^p_{33}). To address the orientation dependence of the interfacial energy, we employ the finite element modeling in Section 4 and consider the bar geometry with different t/w. The boundary constraints chosen are the same as those in Section 4: at the upper surface ($z = L$), the deformations are totally free ($u_1 \neq 0, u_2 \neq 0, u_3 \neq 0$). At the bottom surface ($z = 0$), the deformations are all forbidden ($u_1 = u_2 = u_3 = 0$). Now there is no bulk bending energy in the bar and the strain energy U_{el} equals the interfacial energy U_{front}. Under the condition $\theta_2 = 0°$, the variation of the interfacial energy U_{front} with the orientation angle θ_1 for different

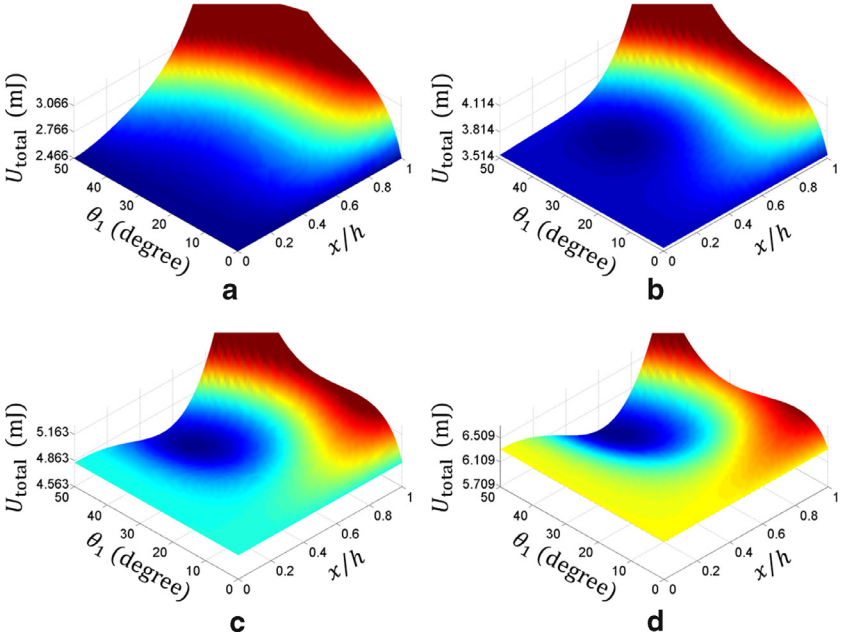

Fig. 15. The variation of total energy U_{total} with two governing parameters x/h and θ_1 for different applied loads: (a) $u/h = 1$, (b) $u/h = 1.2$, (c) $u/h = 1.4$, (d) $u/h = 1.6$.

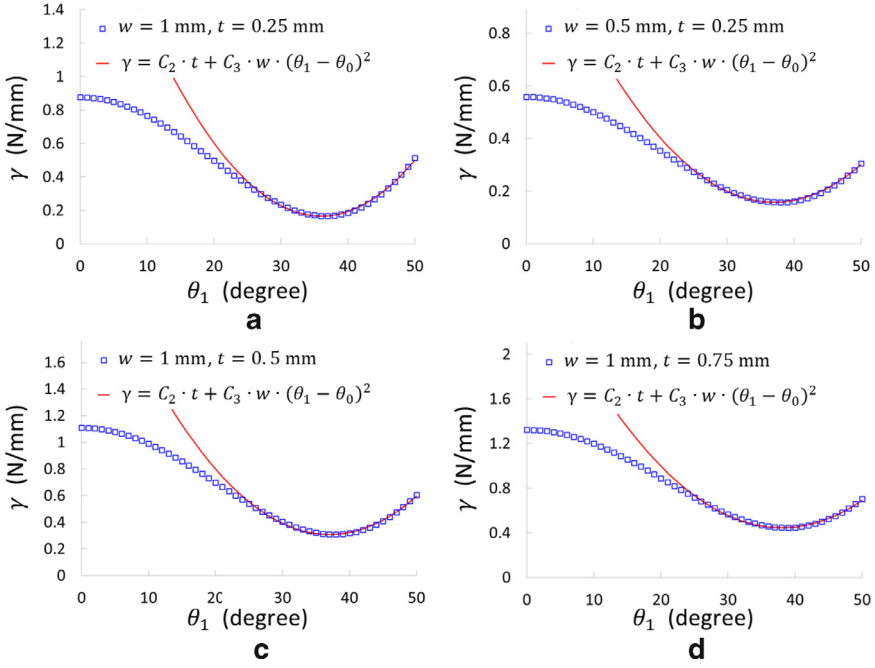

Fig. 16. The variation of front energy density γ with the orientation angles θ_1 (with $\theta_2 = 0$) for four different bar geometries: (a) $w = 1$ mm, $t = 0.25$ mm, (b) $w = 0.5$ mm, $t = 0.25$ mm, (c) $w = 1$ mm, $t = 0.5$ mm, (d) $w = 1$ mm, $t = 0.75$ mm.

combinations of bar width and thickness is shown in Fig. 16. It is seen that we can assume the orientation-dependent interfacial energy to be expressed as:

$$U_{\text{front}} = \gamma \frac{wt}{\cos\theta_1} = \left[C_2 t + C_3 w(\theta_1 - \theta_0)^2\right] \frac{wt}{\cos\theta_1}, \tag{25}$$

where C_2 and C_3 are constants, and C_2 is the same as that in Eq. (22). This scaling relation agrees well with the simulation results for the orientation angle $|\theta_1 - \theta_0| < 15^\circ$.

As a summary, in a more complicated loading condition such as three-point bending the orientation dependence of the interfacial energy density γ can be accounted for by a term proportional to $w(\theta_1 - \theta_0)^2$.

6. Summary and conclusions

The macroscopic interfaces (domain fronts) are commonly observed in the phase transition process of bulk polycrystalline NiTi shape memory alloys under external loading. The understanding and quantification of the interfacial energy are therefore fundamental issues and play important roles in modeling the phase transition process in these materials. In this paper, we studied the energetics of a martensite domain with planar interfaces in a superelastic NiTi bar through an inclusion model. The misfit strain energy due to the presence of a martensite domain was quantified numerically by finite element simulation. It was demonstrated that such misfit energy strongly depends on three length scales (bar length L, width w and thickness t) and also two orientation angles (θ_1 and θ_2) of the interface. Understanding of the physical origin of the interfacial energy as well as its length and orientation dependences was achieved. The main conclusions are as follows:

1. The interfacial energy is a local elastic strain energy stored around the interface. Its physical origin is the interface incompatibility of transformation strain on the interphase boundary. Such incompatibility leads to internal stresses which are long range and spread from the interface to distances of the order of the boundary extent (the smallest dimension of the object).
2. For long NiTi bars under stretching, the interface orientation corresponding to minimum strain energy is always $\theta_1 = \theta_0 \approx 35^\circ$ and $\theta_2 \approx 0^\circ$. In other words, the inter-section of the interface with the front surface (xz-surface) of the bar is the "invariant-line" on that surface, while on the side surface (yz-surface) of the bar it is always perpendicular to the loading axis (z-axis). The interfacial energy density γ per unit area is not a material constant, but shows a linear relationship with a length scale of the bar thickness t.
3. The deviation of interface orientation from the "invariant-line" is a reasonable and observable phenomenon in a more complicated loading condition such as three-point bending. The orientation dependence of the interfacial energy density γ can be accounted for by a term proportional to the square of angle deviation from θ_0, i.e., $(\theta_1 - \theta_0)^2$. This scaling relation agrees well with the simulation results for the orientation angle $|\theta_1 - \theta_0| < 15^\circ$.

Acknowledgment

The financial support from the Hong Kong Research Grants Council (GRF Project No. 619511) and from the 973 Program of China (Project No. 2014CB046902) is gratefully acknowledged.

Appendix A. Solution of inclusion problem

A.1. Sub-problem I

The martensite domain is subject to the traction $p = -E\varepsilon_{22}^p > 0$ on its upper and bottom surfaces to guarantee there is no deformation of the bar as shown in Fig. 4(b). We have

$$\sigma_{33}^{\text{I}} = 0,\ \sigma_{22}^{\text{I}} = p,\ \sigma_{32}^{\text{I}} = 0 \text{ for } x_3 > 0,$$
$$\sigma_{33}^{\text{I}} = \sigma_{22}^{\text{I}} = \sigma_{32}^{\text{I}} = 0 \text{ for } x_3 < 0. \tag{A1}$$

A.2. Sub-problem II

The infinite long bar is subjected to the distributed pressure $p/2$ on its upper and bottom surfaces as shown in Fig. 4(c). We have

$$\sigma_{33}^{\text{II}} = 0,\ \sigma_{22}^{\text{II}} = -\frac{p}{2},\ \sigma_{32}^{\text{II}} = 0. \tag{A2}$$

A.3. Sub-problem III

The same infinite bar is subjected to the distributed traction $p/2$ on the left side and the distributed pressure $p/2$ on the right side as shown in Fig. 4(d). The boundary conditions require that at $x_2 = \pm c$,

$$\sigma_{22}^{\mathrm{III}} = -\frac{p}{2},\ \sigma_{32}^{\mathrm{III}} = 0 \quad \text{for} \quad x_3 > 0,$$
$$\sigma_{22}^{\mathrm{III}} = \frac{p}{2},\ \sigma_{32}^{\mathrm{III}} = 0 \quad \text{for} \quad x_3 < 0. \tag{A3}$$

A standard way to solve this problem is to employ Airy's stress function ϕ. The stress components expressed by ϕ are

$$\sigma_{33} = \frac{\partial^2\phi}{\partial x_2^2},\ \sigma_{22} = \frac{\partial^2\phi}{\partial x_3^2},\ \sigma_{32} = -\frac{\partial^2\phi}{\partial x_3 \partial x_2}, \tag{A4}$$

where ϕ satisfies the bi − harmonic equation

$$\frac{\partial^4\phi}{\partial x_3^4} + 2\frac{\partial^4\phi}{\partial x_3^2 \partial x_2^2} + \frac{\partial^4\phi}{\partial x_2^4} = 0.$$

In order to satisfy the bi-harmonic equation, the stress function ϕ can be assumed to take the form

$$\phi = c^2 \int_0^\infty \left[C_1(k)\cosh\left(\frac{kx_2}{c}\right) + C_2(k)\frac{kx_2}{c}\sinh\left(\frac{kx_2}{c}\right)\right]\sin \times\left(\frac{kx_3}{c}\right)dk. \tag{A5}$$

From Eq. (A4), the stress components can be obtained as

$$\sigma_{33}^{\mathrm{III}} = \int_0^\infty k^2 \left\{ C_1(k)\cosh\left(\frac{kx_2}{c}\right) + C_2(k)\left[2\cosh\left(\frac{kx_2}{c}\right) \times + \frac{kx_2}{c}\sinh\left(\frac{kx_2}{c}\right)\right]\right\}\sin\left(\frac{kx_3}{c}\right)dk,$$
$$\sigma_{22}^{\mathrm{III}} = -\int_0^\infty k^2 \left[C_1(k)\cosh\left(\frac{kx_2}{c}\right) + C_2(k)\frac{kx_2}{c}\sinh\left(\frac{kx_2}{c}\right)\right] \times \sin\left(\frac{kx_3}{c}\right)dk,$$
$$\sigma_{32}^{\mathrm{III}} = -\int_0^\infty k^2 \left\{ C_1(k)\sinh\left(\frac{kx_2}{c}\right) + C_2(k)\left[\sinh\left(\frac{kx_2}{c}\right) + \frac{kx_2}{c}\cosh\left(\frac{kx_2}{c}\right)\right]\right\}\cos\left(\frac{kx_3}{c}\right)dk. \tag{A6}$$

In order to satisfy the lateral boundary condition, the unknown functions should be determined by the following equations:

$$C_1(k)\cosh k + C_2(k)k\sinh k = \frac{p}{\pi k^3},$$
$$C_1(k)\sinh k + C_2(k)(\sinh k + k\cosh k) = 0. \tag{A7}$$

by using the relation

$$\int_0^\infty \frac{\sin\left(\frac{kx_3}{c}\right)}{k}dk = \begin{cases} \frac{\pi}{2}, & \text{for } x_3 > 0 \\ 0, & \text{for } x_3 = 0 \\ -\frac{\pi}{2}, & \text{for} x_3 < 0 \end{cases}.$$

From Eq. (A7) we get

$$C_1(k) = \frac{p}{\pi k^3}\frac{\sinh k + k\cosh k}{\sinh k\cosh k + k},\ C_2(k) = -\frac{p}{\pi k^3}\frac{\sinh k}{\sinh k\cosh k + k}. \tag{A8}$$

Therefore,

$$\sigma_{33}^{\mathrm{III}} = -\frac{p}{\pi}\int_0^\infty \left[\frac{\sinh k - k\cosh k}{\sinh k\cosh k + k}\cosh\left(\frac{kx_2}{c}\right) + \frac{\sinh k}{\sinh k\cosh k + k}\frac{kx_2}{c}\sinh\left(\frac{kx_2}{c}\right)\right]\frac{\sin\left(\frac{kx_3}{c}\right)}{k}dk,$$
$$\sigma_{22}^{\mathrm{III}} = -\frac{p}{\pi}\int_0^\infty \left[\frac{\sinh k + k\cosh k}{\sinh k\cosh k + k}\cosh\left(\frac{kx_2}{c}\right) - \frac{\sinh k}{\sinh k\cosh k + k}\frac{kx_2}{c}\sinh\left(\frac{kx_2}{c}\right)\right]\frac{\sin\left(\frac{kx_3}{c}\right)}{k}dk,$$
$$\sigma_{32}^{\mathrm{III}} = -\frac{p}{\pi}\int_0^\infty \left[\frac{k\cosh k}{\sinh k\cosh k + k}\sinh\left(\frac{kx_2}{c}\right) - \frac{\sinh k}{\sinh k\cosh k + k}\frac{kx_2}{c}\cosh\left(\frac{kx_2}{c}\right)\right]\frac{\cos\left(\frac{kx_3}{c}\right)}{k}dk. \tag{A9}$$

A.4. Superposition

By superposing three sub-problems, the total stresses can be expressed as

$$\sigma_{33} = \sigma_{33}^{\mathrm{I}} + \sigma_{33}^{\mathrm{II}} + \sigma_{33}^{\mathrm{III}} = -\frac{p}{\pi}\int_0^\infty \left[\frac{\sinh k - k\cosh k}{\sinh k\cosh k + k}\cosh\left(\frac{kx_2}{c}\right) + \frac{\sinh k}{\sinh k\cosh k + k}\frac{kx_2}{c}\sinh\left(\frac{kx_2}{c}\right)\right]\frac{\sin\left(\frac{kx_3}{c}\right)}{k}dk,$$
$$\sigma_{22} = \sigma_{22}^{\mathrm{I}} + \sigma_{22}^{\mathrm{II}} + \sigma_{22}^{\mathrm{III}} = \frac{p}{\pi}\int_0^\infty \left[1 - \frac{\sinh k + k\cosh k}{\sinh k\cosh k + k}\cosh\left(\frac{kx_2}{c}\right) + \frac{\sinh k}{\sinh k\cosh k + k}\frac{kx_2}{c}\sinh\left(\frac{kx_2}{c}\right)\right]\frac{\sin\left(\frac{kx_3}{c}\right)}{k}dk,$$
$$\sigma_{32} = \sigma_{32}^{\mathrm{I}} + \sigma_{32}^{\mathrm{II}} + \sigma_{32}^{\mathrm{III}} = -\frac{p}{\pi}\int_0^\infty \left[\frac{k\cosh k}{\sinh k\cosh k + k}\sinh\left(\frac{kx_2}{c}\right) - \frac{\sinh k}{\sinh k\cosh k + k}\frac{kx_2}{c}\cosh\left(\frac{kx_2}{c}\right)\right]\frac{\cos\left(\frac{kx_3}{c}\right)}{k}dk. \tag{A10}$$

Specifically when $x_2 = 0$, we have

$$\sigma_{33} = -\frac{p}{\pi}\int_0^\infty \left\{\frac{\sinh k - k\cosh k}{\sinh k\cosh k + k}\right\}\frac{\sin\left(\frac{kx_3}{c}\right)}{k}dk,$$
$$\sigma_{22} = \frac{p}{\pi}\int_0^\infty \left[1 - \frac{\sinh k + k\cosh k}{\sinh k\cosh k + k}\right]\frac{\sin\left(\frac{kx_3}{c}\right)}{k}dk,$$
$$\sigma_{32} = 0. \tag{A11}$$

The total elastic energy of the bar can be calculated as

$$U_{\mathrm{el}} = \frac{1}{2}\int_V \sigma_{ij}\varepsilon_{ij}^e dV = \frac{E\left(\varepsilon_{22}^p\right)^2 c}{\pi}\int_0^\infty \left\{\int_0^\infty \left[1 - \frac{2\sinh k\sinh k}{\sinh k\cosh k + k}\frac{1}{k}\right]\frac{\sin\left(\frac{kx_3}{c}\right)}{k}dk\right\}dx_3. \tag{A12}$$

References

Bhattacharya, K., 2003. Microstructure of Martensite. Oxford University Press, Oxford.

Boyko, V.S., Garber, R.I., Kossevich, A.M., 1994. Reversible Crystal Plasticity. AIP Press, Woodbury, NY.

Cahn, J.W., Hilliard, J.E., 1958. Free energy of a nonuniform system I. Interfacial free energy. J. Chem. Phys. 28, 258–267.

Cahn, J.W., 1961. On spinodal decomposition. Acta Metallurgica 9, 795–801.

Corona, E., Iadicola, M., Shaw, J., 2002. Buckling of steel bars with Lüders bands. Int. J. Solids Struct. 39, 3313–3336.

Dai, H.H., Cai, Z.X., 2006. Phase transitions in a slender cylinder composed of an incompressible elastic material. I. Asymptotic model equation. Proceedings of the Royal Society A 462, 75–95.

Dong, L., Sun, Q.P., 2009. Stress hysteresis and domain evolution in thermoelastic tension strips. Acta Mechanica Solida Sinica 22, 399–406.

Dong, L., Sun, Q.P., 2012. On equilibrium domains in superelastic NiTi tubes – helix versus cylinder. Int. J. Solids Struct. 49, 1063–1076.

Falk, F., 1983. Ginzburg–Landau theory of static domain-walls in shape-memory alloys. Z. Phys. B Conden. Matter 51, 177–185.

Feng, P., Sun, Q.P., 2006. Experimental investigation on macroscopic domain formation and evolution in polycrystalline NiTi microtubing under mechanical force. J. Mech. Phys. Solids 54, 1568–1603.

He, Y.J., Sun, Q.P., 2009. Non-local modeling on macroscopic domain patterns in phase transformation of NiTi tubes. Acta Mechanica Solida Sinica 22, 407–417.

He, Y.J., Sun, Q.P., 2009. Effects of structural and material length scales on stress-induced martensite macro-domain patterns in tube configurations. Int. J. Solids Struct. 46, 3045–3060.

He, Y.J., Sun, Q.P., 2009. Scaling relationship on macroscopic helical domains in NiTi tubes. Int. J. Solids Struct. 46, 4242–4251.

He, Y.J., Sun, Q.P., 2010. Macroscopic equilibrium domain structure and geometric compatibility in elastic phase transition of thin plates. Int. J. Mech. Sci. 52, 198–211.

Khachaturyan, A.G., 1983. Theory of Structural Transformations in Solids. Wiley, NY.

Li, Z.Q., Sun, Q.P., 2002. The initiation and growth of macroscopic martensite band in nano-grained NiTi microtube under tension. Int. J. Plast. 18, 1481–1498.

Maciejewski, G., Stupkiewicz, S., Petryk, H., 2005. Elastic micro-strain energy at the austenite-twinned martensite interface. Arch. Mech. 57, 277–297.

Mura, T., 1987. Micromechanics of Defects in Solids. Martinus Nijhoff, Dordrecht.

Porter, D.A., Easterling, K.E., Sherif, M.Y., 2009. Phase Transformations in Metals and Alloys, 3rd ed. CRC Press, Boca Raton, FL.

Roitburd, A.L., 1969. Domain structure of crystals formed in a solid phase. Soviet Phys. - Solid State 10, 2870–2876.

Roitburd, A.L., 1974. The theory of the formation of a heterophase structure in phase transformations in solids. Soviet Phys Uspekhi 17, 326–344.

Roitburd, A.L., 1978. Martensitic transformation as a typical phase transformation in solids. Solid State Phys 33, 317–390.

Roitburd, A.L., 1998. Thermodynamics of polydomain heterostructures: II. Effect of microstresses. J Appl Phys 83, 239–245.

Shaw, J.A., Kyriakides, S., 1997. On the nucleation and propagation of phase transformation fronts in a NiTi alloy. Acta Mater 45, 673–700.

Shaw, J.A., Kyriakides, S., 1998. Initiation and propagation of localized deformation in elasto-plastic strips under uniaxial tension. Int J Plast. 43, 837–871.

Shaw, J.A., 2000. Simulations of localized thermo-mechanical behavior in a NiTi shape memory alloy.

Sun, Q.P., Li, Z.Q., 2002. Phase transformation in superelastic NiTi polycrystalline microtubes under tension and torsion-from localization to homogeneous deformation. Int. J. Solids Struct. 39, 3797–3809.

Zhang, X.H., Feng, P., He, Y.J., Yu, T.X., Sun, Q.P., 2010. Experimental study on rate dependence of macroscopic domain and stress hysteresis in NiTi shape memory alloy strips. Int. J. Mech. Sci. 52, 1660–1670.

Zhou, R.H., 2011. Ph.D. Thesis. Macroscopic domain pattern selection in shape memory alloys: effects of length and time scales. The Hong Kong University of Science and Technology.

Zhou, R.H., Sun, Q.P., 2011. Helical domain patterns in tube configurations: effect of geometry length scales. Solid State Phenom. 172-174, 1090–1095.